

2022

## S-Type Stars: LaO Line List for the $B^2\Sigma^+-X^2\Sigma^+$ Band System

P. F. Bernath

*Old Dominion University*, pbernath@odu.edu

Randika Dodangodage

*Old Dominion University*, rdodango@odu.edu

J. Liévin

Follow this and additional works at: [https://digitalcommons.odu.edu/chemistry\\_fac\\_pubs](https://digitalcommons.odu.edu/chemistry_fac_pubs)



Part of the [Inorganic Chemistry Commons](#), [Physical Chemistry Commons](#), and the [Stars, Interstellar Medium and the Galaxy Commons](#)

---

### Original Publication Citation

Bernath, P.F., Dodangodage, R., Liévin, J. (2022) S-type stars: LaO line list for the  $B^2\Sigma^+-X^2\Sigma^+$  band system. *The Astrophysical Journal*, 933 (1) 1-7, Article 99. <https://doi.org/10.3847/1538-4357/ac731f>

This Article is brought to you for free and open access by the Chemistry & Biochemistry at ODU Digital Commons. It has been accepted for inclusion in Chemistry & Biochemistry Faculty Publications by an authorized administrator of ODU Digital Commons. For more information, please contact [digitalcommons@odu.edu](mailto:digitalcommons@odu.edu).



# S-type Stars: LaO Line List for the $B^2\Sigma^+-X^2\Sigma^+$ Band System

P. F. Bernath<sup>1,2</sup>, R. Dodangodage<sup>2</sup>, and J. Liévin<sup>3</sup><sup>1</sup> Department of Chemistry and Biochemistry, Old Dominion University, Norfolk, VA 23529, USA<sup>2</sup> Department of Physics, Old Dominion University, Norfolk, VA 23529, USA; [rdodango@odu.edu](mailto:rdodango@odu.edu)<sup>3</sup> Université Libre de Bruxelles, Spectroscopy, Quantum Chemistry and Atmospheric Remote Sensing, CP 160/09, Av. F. D. Roosevelt 50, Bruxelles, Belgium

Received 2022 March 10; revised 2022 May 16; accepted 2022 May 23; published 2022 July 6

## Abstract

LaO bands are a characteristic feature in the spectrum of cool S-type stars. La is made primarily by the *s*-process during the asymptotic giant branch phase of stellar evolution. The  $B^2\Sigma^+-X^2\Sigma^+$  and  $A^2\Pi-X^2\Sigma^+$  band systems can be used to determine the La abundances in cool S stars. The bands of the  $B^2\Sigma^+-X^2\Sigma^+$  with  $v'$  and  $v'' \leq 5$  have been rotationally analyzed from an emission spectrum from a carbon furnace. Line strengths are calculated using an ab initio transition dipole function, corrected using experimental lifetimes. We provide a line list for the  $B^2\Sigma^+-X^2\Sigma^+$  band system that can be used to determine La abundances.

*Unified Astronomy Thesaurus concepts:* Spectral line lists (2082); Laboratory astrophysics (2004)

*Supporting material:* data behind figure, machine-readable tables

## 1. Introduction

The formation of the elements is an active area of research (Johnson 2019). For example, the important role of neutron star mergers in the synthesis of heavy elements has recently become evident (Ji et al. 2019). Lanthanum (La) is formed both in the rapid neutron-capture process (*r*-process) in kilonovae from neutron star mergers and in the slow neutron-capture process (*s*-process) in asymptotic giant branch (AGB) stars (Johnson 2019). The *s*-process is thought to be responsible for the synthesis of about half of the elements heavier than Fe (Neyskens et al. 2015). The *s*-process can be studied by measuring the stellar abundance of heavy elements such as Y, Zr, Ba, and La that are formed from lighter elements by the repeated absorption of a neutron followed by  $\beta$ -decay. For hot stars using atomic  $La^+$  ions (e.g., La II 4921.778 Å) for abundance measurements is convenient, but for cooler objects, the visible and near-infrared electronic transitions of LaO are more useful (MacConnell et al. 2000).

The *s*-process takes place in the late AGB phase of stellar evolution when most of the hydrogen has been consumed (Wallerstein et al. 1997). Helium and hydrogen burning occur in thin shells around a C/O core and thermal pulses dredge up carbon and other elements. The stellar surface becomes increasingly rich in carbon, ultimately forming a carbon star. S stars have carbon abundances approximately equal to their oxygen abundances and display spectral features associated with *s*-process elements, e.g., LaO bands from the  $B^2\Sigma^+-X^2\Sigma^+$  and  $A^2\Pi-X^2\Sigma^+$  transitions. LaO line lists are needed to determine La abundances in cool S-type stars. The goal of our work is to provide a modern line list for the  $B^2\Sigma^+-X^2\Sigma^+$  band system of LaO for this purpose.

LaO has four low-lying electronic states:  $X^2\Sigma^+$ ,  $A^2\Delta$ ,  $A^2\Pi$ , and  $B^2\Sigma^+$ . The green  $B^2\Sigma^+-X^2\Sigma^+$  transition and the very red  $A^2\Pi-X^2\Sigma^+$  transition have been studied many times (Bacis et al. 1973; Bernard & Sibai 1980; Bernard et al. 1999) and the  $A^2\Pi-A^2\Delta$  emission bands can be seen near 2  $\mu$ m in the near-infrared (Bernard & Vergès 2000). The rotational lines of the A–X and

B–X electronic transitions are doubled with a splitting of about  $0.5 \text{ cm}^{-1}$ . This unusual feature caused considerable confusion until Weltner et al. (1967) assigned the splitting to large magnetic hyperfine structure (hfs) in the  $X^2\Sigma^+$  state due to the  $^{139}\text{La}$  nucleus. Childs et al. (1986) studied the hfs in the  $X^2\Sigma^+$  and  $B^2\Sigma^+$  states with great precision by laser-radio frequency double resonance in a molecular beam. Ground-state microwave spectroscopy has also been carried out (Törring et al. 1988; Suenram et al. 1990). Steimle & Virgo (2002) measured the dipole moments in the  $X^2\Sigma^+$ ,  $A^2\Pi$ , and  $B^2\Sigma^+$  states and analyzed the hfs in the  $A^2\Pi$  state.

Radiative lifetimes for the  $B^2\Sigma^+$  state have been measured by laser-induced fluorescence (Liu & Parson 1977; Carette & Bencheikh 1994). Finally, there are several ab initio calculations of LaO molecular properties (Schamps et al. 1995; Moriyama et al. 2010; Korek et al. 2013).

We report a reanalysis of the  $B^2\Sigma^+-X^2\Sigma^+$  band system up to  $v = 5$  in both ground and excited states. Using an ab initio transition dipole moment function, scaled with experimental data, we have calculated the line strengths and provide a line list suitable for the simulation of stellar spectra.

## 2. Experiment

The emission spectrum of LaO was recorded in 1988 using a carbon tube furnace (King furnace) with the McMath-Pierce 1 m Fourier transform spectrometer at the National Solar Observatory at Kitt Peak in Arizona. The data are available from the National Solar Observatory Digital Library as file 881025-03. The furnace had a temperature of 2100°C. The spectrometer was operated with silicon diode detectors and covered the nominal range of 350–1100 nm set by the visible beamsplitter and the silicon diodes. Eight scans were recorded in about 1 hr at a spectral resolution of  $0.05 \text{ cm}^{-1}$ .

An overview spectrum of the  $\Delta v = 1$  sequence of the  $B^2\Sigma^+-X^2\Sigma^+$  transition is provided in Figure 1. Figure 2 shows the spectrum near the 1–0 band heads. The calculation of the simulated spectra in the two figures is discussed below.

## 3. Ab Initio Calculations

The electric transition dipole moment (TDM) curve for the  $B^2\Sigma^+-X^2\Sigma^+$  transition has been calculated using the MOLPRO

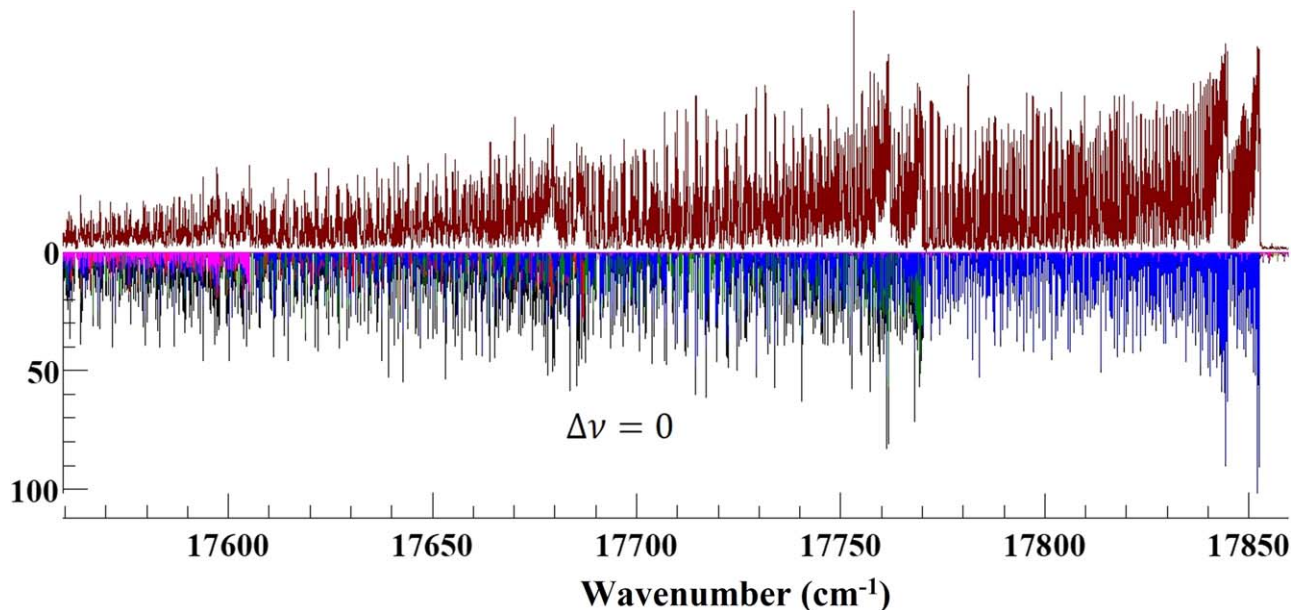


**Figure 1.** Overview emission spectrum of LaO (above) and simulation (below) of the  $\Delta\nu = 0$  sequence of the  $B^2\Sigma^+-X^2\Sigma^+$  transition. (Blue: 0-0 band, green: 1-1 band, red: 2-2 band, and pink: 3-3 band.)

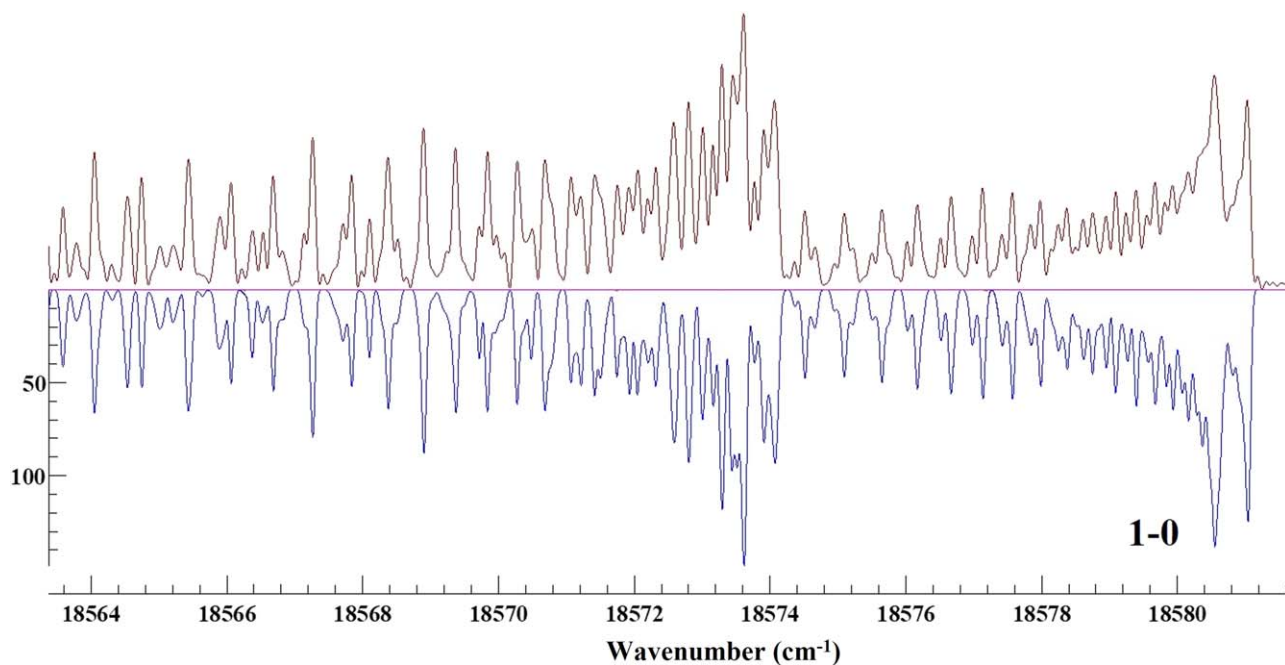


**Figure 2.** The spectrum of LaO (above) and simulation (below) of the B-X 1-0 band.

Quantum Chemistry package (Werner et al. 2012, 2019). These calculations were performed with the internally contracted configuration interaction method (ic-MRCI; Knowles & Werner 1988; Werner & Knowles 1988), using molecular orbitals optimized by means of state-averaged complete active space self-consistent field (SA-CASSCF) calculations (Knowles & Werner 1985; Werner & Knowles 1985). The state averaging has been applied to the  $X^2\Sigma^+(A_1)$ ,  $A'^2\Delta(A_1+A_2)$ , and  $B^2\Sigma^+(A_1)$  states, sharing the same  $A_1$  symmetry of the  $C_{2v}$  subgroup used by MOLPRO. Davidson's correction for unlinked clusters (Langhoff & Davidson 1974), adapted to a relaxed reference (Werner et al. 2008), has been taken into account in the energy calculations. The active space contains five  $\sigma$ , three  $\pi$ , and one  $\delta$  molecular orbitals,

correlating to the lanthanum 6s, 6p, and 5d and oxygen 2p atomic orbitals. Seven electrons are distributed in all possible ways in this active space, according to the spatial and spin symmetries of the calculated states. A quasirelativistic Wood-Boring energy-adjusted electron core potential (ECP) has been used for describing the 46 core electrons ( $Kr + 4d^{10}$ ) of the lanthanum atom (Dolg et al. 1989). The corresponding spd basis set has been used (Dolg et al. 1989), augmented by an uncontracted set of three f Gaussian functions (Weigand et al. 2009). The scalar relativistic effects taken into account by the ECP are essential for describing a system containing a heavy element like lanthanum, as shown by the atomic and molecular test calculations provided in the above referenced papers. Dunning's aug-cc-pVQZ correlation-consistent basis set

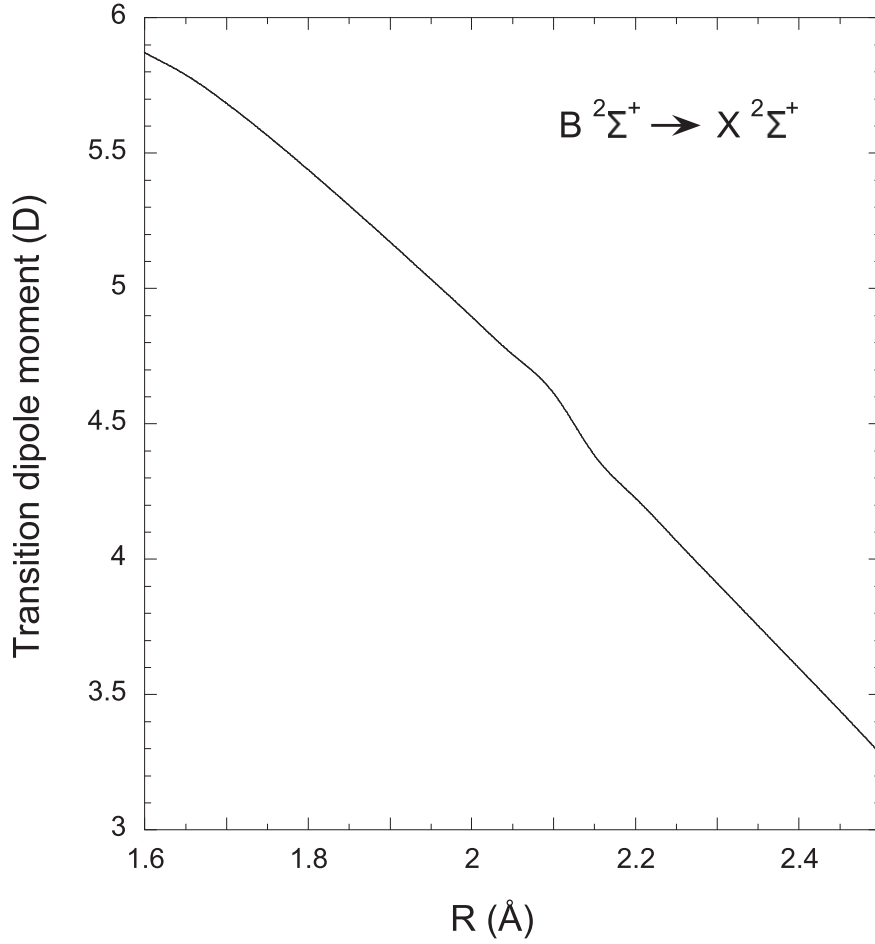


**Figure 3.** Ab initio transition dipole moment curve for the  $B^2\Sigma^+ - X^2\Sigma^+$  transition of LaO. (The data used to create this figure are available.)

(Dunning 1989; Kendall et al. 1992) has been adopted for the oxygen atom. The term energy values,  $T_e$ , for the A' and B states are calculated to be 8189 and 18,121  $\text{cm}^{-1}$ , respectively, in agreement with the corresponding experimental values of 7844.1 (Bernard & Vergès 2000) and 17,878.7  $\text{cm}^{-1}$  (Bernard et al. 1999). The calculations have been carried out at a set of internuclear distances,  $R$ , ranging from 1.6 to 2.5 Å, by steps of 0.05 Å, and the resulting TDM curve has been interpolated by  $B$ -splines to create a set of 1592 points on the same  $R$  range. The calculated points and the interpolated points are provided as supplementary data. This curve is shown in Figure 3. The inflection point at 2.15 Å results from an interaction between the two higher  $\pi$  orbitals of the active space. This transition function has not been predicted in previous ab initio works.

#### 4. Line Positions

The  $B^2\Sigma^+ - X^2\Sigma^+$  transition of LaO was rotationally analyzed using the PGOPHER program (Western 2017) with the experimental spectrum used as an overlay. The rotational structure of the LaO  $^2\Sigma^+$  states can be described by the standard  $N^2$  Hamiltonian ( $H_{\text{rot}}$ ), where  $N$  is the rotational angular momentum ( $N = J - S$ ),  $J$  is the total angular momentum excluding nuclear spin,  $S$  is the total electron spin,  $B$  is the rotational constant, and  $D$  and  $H$  are the centrifugal

distortion constants (Brown & Carrington 2003):

$$H_{\text{rot}} = BN^2 - DN^4 + HN^6. \quad (1)$$

The spin-rotation (electron spin, molecular rotation) interaction of LaO is described by  $H_{\text{sr}}$ , where  $\gamma$  is the spin-rotation constant, and  $\gamma_D$  is the centrifugal distortion correction:

$$H_{\text{sr}} = \gamma N \cdot S + \gamma_D N \cdot S(N^2). \quad (2)$$

$^{139}\text{La}$  has a nuclear spin ( $I$ ) of 7/2 (100% natural abundance), and the interaction of nuclear spin with the total angular momentum ( $J$ ) gives rise to the nuclear hfs  $F = J + I$  of LaO. This hfs can be modeled using the Froeh and Foley constants (Frosch & Foley 1952) and the Hamiltonian for the hfs ( $H_{\text{hfs}}$ ) can be written as (Childs et al. 1986; Törring et al. 1988; Steimle & Virgo 2002; Brown & Carrington 2003)

$$H_{\text{hfs}} = bI \cdot S + cI_z S_z + C_I I \cdot N + eqQ \frac{3I_z^2 - I(I+1)}{4I(2I-1)}, \quad (3)$$

in which  $b$  is the Fermi contact constant,  $c$  is the dipole-dipole interaction constant,  $C_I$  is the nuclear spin-rotation interaction constant, and  $eqQ$  is the nuclear quadrupole coupling constant.

**Table 1**  
Spectroscopic Parameters for the  $X^2\Sigma^+$  State

|                       | $v = 0$                  | $v = 1$                  | $v = 2$                  | $v = 3$                  | $v = 4$                  | $v = 5$                  |
|-----------------------|--------------------------|--------------------------|--------------------------|--------------------------|--------------------------|--------------------------|
| $T_v$                 | 0 <sup>a</sup>           | 812.73754(70)            | 1621.19342(72)           | 2425.35172(82)           | 3225.18499(94)           | 4020.6780(12)            |
| $B_v$                 | 0.351807477 <sup>a</sup> | 0.350377881 <sup>a</sup> | 0.348942339 <sup>a</sup> | 0.347500853 <sup>a</sup> | 0.346053423 <sup>a</sup> | 0.344600047 <sup>a</sup> |
| $10^7 D_v$            | 2.6246 <sup>a</sup>      | 2.6224 <sup>a</sup>      | 2.6201 <sup>a</sup>      | 2.61788 <sup>a</sup>     | 2.61561 <sup>a</sup>     | 2.6133 <sup>a</sup>      |
| $10^3 \gamma_v$       | 2.2081 <sup>b</sup>      | 2.22181 <sup>b</sup>     | 2.23685 <sup>b</sup>     | 2.25321 <sup>b</sup>     | 2.2709 <sup>b</sup>      | 2.28992 <sup>b</sup>     |
| $10^8 \gamma_{Dv}$    | -1.45734 <sup>b</sup>    | -1.43666 <sup>b</sup>    | -1.41598 <sup>b</sup>    | -1.3953 <sup>b</sup>     | -1.3746 <sup>b</sup>     | -1.3539 <sup>b</sup>     |
| $10^{14} \gamma_{Hv}$ | 4.4364 <sup>b</sup>      |
| $b$                   | 0.121147 <sup>b</sup>    | 0.121232 <sup>b</sup>    | 0.121317 <sup>b</sup>    | 0.121401 <sup>b</sup>    | 0.1214860 <sup>b</sup>   | 0.121571 <sup>b</sup>    |
| $10^3 c$              | 3.1596 <sup>b</sup>      | 3.18 <sup>b</sup>        | 3.200 <sup>b</sup>       | 3.2208 <sup>b</sup>      | 3.2412 <sup>b</sup>      | 3.2617 <sup>b</sup>      |
| $10^3 eqQ$            | -2.8131 <sup>b</sup>     | -2.807 <sup>b</sup>      | -2.8017 <sup>b</sup>     | -2.7961 <sup>b</sup>     | -2.7904 <sup>b</sup>     | -2.7847 <sup>b</sup>     |
| $10^7 C_I$            | 4.818 <sup>b</sup>       |
| $10^8 b_D$            | 2.66851 <sup>b</sup>     |
| $10^9 c_D$            | 6.2543 <sup>b</sup>      |
| $10^8 eqQ_D$          | -1.4777 <sup>b</sup>     |

**Notes.** One standard deviation is given in parenthesis. All values are in  $\text{cm}^{-1}$ .

<sup>a</sup> Held fixed during fitting. Values are from Dunham constants of Törring et al. (1988).

<sup>b</sup> Held fixed during fitting. Values are from Childs et al. (1986).

The effective Hamiltonian ( $H_{\text{eff}}$ ) for LaO  $^2\Sigma^+$  states is thus

$$H_{\text{eff}} = H_{\text{rot}} + H_{\text{sr}} + H_{\text{hfs}}. \quad (4)$$

In the upper state ( $B^2\Sigma^+$ ), the spin  $S$  of the unpaired electron couples with the rotational angular momentum  $N$  ( $\mathbf{J} = \mathbf{N} + \mathbf{S}$ ) and spin-rotation constant is known to be negative, so  $J = N - 1/2$  ( $F_2$ ) lies higher and  $J = N + 1/2$  ( $F_1$ ) lies lower ( $S = 1/2$  for a doublet state). The resulting  $\mathbf{J}$  couples with the nuclear spin  $\mathbf{I}$  ( $I = 0$  for  $^{16}\text{O}$ ) to form up to eight ( $2I + 1$ ) hyperfine levels ( $\mathbf{F} = \mathbf{J} + \mathbf{I}$ ) known as  $b_{\beta J}$  coupling (Bacis et al. 1973; Brown & Carrington 2003).

For the ground state ( $X^2\Sigma^+$ ), the Fermi contact parameter  $b$  is larger than the spin-rotation interaction. Therefore, it is convenient to couple the nuclear spin  $\mathbf{I}$  and the electron spin  $\mathbf{S}$  to form an intermediate angular momentum  $\mathbf{G} = \mathbf{I} + \mathbf{S}$ . All rotational levels then split into two components,  $G = 4$ , which lies higher, and  $G = 3$ , which lies lower. Each  $\mathbf{G}$  level couples with rotational angular momentum  $N$ , which forms up to  $2G + 1$  hyperfine levels. This type of coupling  $\mathbf{F} = \mathbf{G} + \mathbf{N}$  is known as  $b_{\beta S}$  coupling (Bacis et al. 1973; Brown & Carrington 2003). The  $G = 4$  to  $G = 3$  splitting is about  $0.52 \text{ cm}^{-1}$  and is responsible for the unusual doubling of the lines.

The vibrational and rotational dependence of these interactions can be taken into account by expanding each quantity ( $X_{i,j}$ ) in a Dunham-type power series,

$$X_{v,N} = \sum_{i,j} X_{i,j} \left( v + \frac{1}{2} \right)^i [N(N+1)]^j. \quad (5)$$

Using this expansion Childs et al. (1986) were able to determine the  $v$  dependence of the hfs and spin-rotation constants for both  $X^2\Sigma^+$  and  $B^2\Sigma^+$  states. Since their constants are more precise than can be obtained from our experiment, the hfs constants determined by Childs et al. (1986) were used in our analysis to calculate the constants up to  $v = 5$  in both  $X^2\Sigma^+$  and  $B^2\Sigma^+$  states and were held fixed during the fitting. In addition, the spin-rotation constants of Childs et al. (1986) were used to calculate these parameters for the ground state. The calculated values are given in Tables 1 and 2.

Törring et al. (1988) have obtained a precise set of rotational constants for  $v = 0-2$  of the  $X^2\Sigma^+$  state by microwave spectroscopy.  $B_v$  and  $D_v$  for the  $X^2\Sigma^+$  state vibrational levels up to  $v = 5$  were calculated using Equations (6) and (7), and

were fixed for the  $X^2\Sigma^+$  state (Table 1):

$$B_v = B_e - \alpha_e \left( v + \frac{1}{2} \right) + \gamma_e \left( v + \frac{1}{2} \right)^2, \quad (6)$$

$$D_v = D_e + \beta_e \left( v + \frac{1}{2} \right). \quad (7)$$

Bernard et al. (1999) obtained equilibrium spectroscopic constants for both  $X^2\Sigma^+$  and  $B^2\Sigma^+$  states. We used the equilibrium constants from Bernard et al. (1999) to calculate the starting values for the origins of the  $X^2\Sigma^+$  and  $B^2\Sigma^+$  vibrational levels for  $v = 0$  to  $v = 5$ . The initial values of  $B_v$ ,  $D_v$ , and  $\gamma_v$  for the  $B^2\Sigma^+$  state were also calculated from the spectroscopic constants given in Bernard et al. (1999). The final fitted values for the spectroscopic constants and all constants held fixed in the  $X^2\Sigma^+$  and  $B^2\Sigma^+$  states are given in Tables 1 and 2. The associated matrix elements for the Hamiltonian used in the fitting are available from PGOPHER (Western 2017).

In the analysis, 12,120 lines were assigned in the 2-0, 3-1, 4-2, 5-3, 1-0, 2-1, 3-2, 4-3, 5-4, 0-0, 1-1, 2-2, 3-3, 4-4, 5-5, 0-1, 1-2, 2-3, 3-4, 4-5, 0-2, 1-3, 2-4, and 3-5 bands. Maximum  $J''$  values are 120.5, 131.5, 120.5, 125.5, 93.5, and 89.5 for  $v'' = 0, 1, 2, 3, 4, 5$ , respectively. A sample of the observed and calculated line list is given in Table 3. The labeling for the lines provided in Table 3 is  $\Delta^N \Delta J_{(F')F_j''} (J'') F', F''$ , in which  $N$  is the quantum number for rotational angular momentum,  $J$  is the quantum number for total angular momentum exclusive of nuclear spin, and  $F'_i, F_j''$ , and  $F$ ; subscripted  $F_{i,j}$  are the customary labels for the two spin components of a  $^2\Sigma^+$  states, 1 has  $J = N + 1/2$  and 2 has  $J = N - 1/2$ , and the trailing  $F'$  and  $F''$  values are the total angular momentum including nuclear spin. As usual, primes are for the upper B state, and double primes are for the lower X state.

## 5. Line Strengths and Line Lists

The calculation of line strengths is based on the ab initio transition dipole moment and RKR potential curves. The inputs for Le Roy's RKR program (Le Roy 2017a) are the customary

**Table 2**  
Spectroscopic Constants for the  $B^2\Sigma^+$  State

|                    | $v = 0$            | $v = 1$             | $v = 2$             | $v = 3$            | $v = 4$            | $v = 5$            |
|--------------------|--------------------|---------------------|---------------------|--------------------|--------------------|--------------------|
| $T_v$              | 17837.3937(17)     | 18567.6509(13)      | 19293.8973(14)      | 20016.1283(14)     | 20734.2972(21)     | 21448.3950(39)     |
| $B_v$              | 0.34055994(56)     | 0.33902396(38)      | 0.33748655(53)      | 0.33594209(46)     | 0.3343991(11)      | 0.3328452(22)      |
| $10^7 D_v$         | 2.93981(39)        | 2.93253(23)         | 2.92742(40)         | 2.92026(33)        | 2.9266(13)         | 2.9182(25)         |
| $\gamma_v$         | -0.253556(35)      | -0.253450(25)       | -0.253252(30)       | -0.253266(25)      | -0.253778(31)      | -0.253434(51)      |
| $10^7 \gamma_{Dv}$ | -2.674(40)         | -2.624(26)          | -2.666(39)          | -2.390(33)         | ...                | ...                |
| $10^2 b$           | 1.94 <sup>a</sup>  | 1.905 <sup>a</sup>  | 1.871 <sup>a</sup>  | 1.837 <sup>a</sup> | 1.802 <sup>a</sup> | 1.768 <sup>a</sup> |
| $10^3 c$           | 6.409 <sup>a</sup> | 5.939 <sup>a</sup>  | 5.469 <sup>a</sup>  | 4.998 <sup>a</sup> | 4.528 <sup>a</sup> | 4.058 <sup>a</sup> |
| $10^3 eqQ$         | -6.56 <sup>a</sup> | -6.776 <sup>a</sup> | -6.993 <sup>a</sup> | -7.21 <sup>a</sup> | -7.43 <sup>a</sup> | -7.64 <sup>a</sup> |

**Notes.** One standard deviation is given in parentheses. All values are in  $\text{cm}^{-1}$ .

<sup>a</sup> Held fixed during fitting. Values are from Childs et al. (1986).

**Table 3**  
Sample of Observed and Calculated Line List of the B–X Transition

| $F'$ | $p'$ | $F''$ | $p''$ | Obs ( $\text{cm}^{-1}$ ) | Calc ( $\text{cm}^{-1}$ ) | Obs-Calc ( $\text{cm}^{-1}$ ) | Line Assignment  |
|------|------|-------|-------|--------------------------|---------------------------|-------------------------------|--|
| 55   | f    | 54    | f     | 17849.6052               | 17849.6233                | -0.0181                       | rR2(50.5)55,54 : B $v = 0$ 51.5 52 F2f 55—X $v = 0$ 50.5 51 F2f 54 |
| 47   | e    | 46    | e     | 17849.6052               | 17849.5800                | 0.0252                        | rR2(49.5)47,46 : B $v = 0$ 50.5 51 F2f 47—X $v = 0$ 49.5 50 F2f 46 |
| 54   | e    | 53    | e     | 17849.6052               | 17849.6214                | -0.0162                       | rR2(50.5)54,53 : B $v = 0$ 51.5 52 F2f 54—X $v = 0$ 50.5 51 F2f 53 |
| 48   | f    | 47    | f     | 17849.6052               | 17849.5533                | 0.0519                        | rR2(49.5)48,47 : B $v = 0$ 50.5 51 F2f 48—X $v = 0$ 49.5 50 F2f 47 |
| 53   | f    | 52    | f     | 17849.6052               | 17849.6187                | -0.0135                       | rR2(50.5)53,52 : B $v = 0$ 51.5 52 F2f 53—X $v = 0$ 50.5 51 F2f 52 |

**Note.**  $F'$  and  $F''$  are the total angular momentum of the B and X states, respectively.  $p$  is the parity. Obs is the observed line position in  $\text{cm}^{-1}$ ; Calc is the calculated line position in  $\text{cm}^{-1}$ ; Obs-Calc is the difference of observed and calculated line position in  $\text{cm}^{-1}$ . Line assignment illustrates the transition  ${}^{\Delta N} \Delta J_{(F')F''}(J'')F', F'' : B v J' N' F1p/F2p F' - X v J'' N'' F1p/F2p F''$ .

(This table is available in its entirety in machine-readable form.)

$B_v$  (Equation (6)) and  $G_v$  expressions:

$$G_v = \omega_e \left( v + \frac{1}{2} \right) - \omega_e x_e \left( v + \frac{1}{2} \right)^2 + \omega_e y_e \left( v + \frac{1}{2} \right)^3. \quad (8)$$

The rotational constants and band origins in Tables 1 and 2 were fitted to determine the equilibrium constants in Table 4. The equilibrium rotational constants for the ground state are those of Törring et al. (1988). The two RKR potentials and the transition dipole moment functions were input into Le Roy's LEVEL program (Le Roy 2017b), and the transition dipole matrix elements  $\langle \psi_{e',v'} | \mu | \psi_{e'',v''} \rangle$  for  $R(0)$  were calculated (Table 5) for all bands with  $v'$  and  $v'' \leq 5$ . These values were used as the band strengths in PGOPHER. The line list was computed with PGOPHER for  $J < 200$  (Table 6). Although the predicted line positions are increasing unreliable for  $J$  values beyond the maximum value observed, they provide opacity for low-resolution astronomical applications. The bond dissociation energy of LaO in the  $X^2\Sigma^+$  state used in the LEVEL calculation was  $782 \pm 21 \text{ kJ mol}^{-1}$  ( $65,370 \text{ cm}^{-1}$ ; Darwent 1970).

The Einstein  $A_{v' \rightarrow v''}$  ( $\text{s}^{-1}$ ) values were calculated using  $A_{v' \rightarrow v''} = 3.136 \times 10^{-7} \nu^3 \mu_{v' \rightarrow v''}^2$  (Bernath 2020), where  $\nu$  is the band origin for the B–X  $v' \rightarrow v''$  transition in  $\text{cm}^{-1}$  and  $\mu_{v' \rightarrow v''}$  is the transition moment (debye) given in Table 5, corrected by a factor of 0.77. The lifetime  $\tau$  is calculated using all radiative rates connecting the upper vibrational level ( $v'$ ) to all lower vibrational levels ( $v''$ ):

$$\tau_{v'} = \frac{1}{\sum_{v''} A_{v' \rightarrow v''}}. \quad (9)$$

The radiative lifetime of the  $B^2\Sigma^+$  state is expected to be in the 20–40 ns range (Liu & Parson 1977), since LaO is isoelectronic to the alkaline earth monohalides for which lifetimes have been determined by Dagdigian et al. (1974).

**Table 4**  
Equilibrium Constants of LaO for the  $X^2\Sigma^+$  and  $B^2\Sigma^+$  States<sup>a</sup>

|                     | $X^2\Sigma^+$            | $B^2\Sigma^+$ |
|---------------------|--------------------------|---------------|
| $\omega_e$          | 816.9969(25)             | 734.2344(78)  |
| $\omega_e x_e$      | 2.1243(11)               | 1.9830(36)    |
| $10^3 \omega_e y_e$ | -3.48(13)                | -4.09(45)     |
| $B_e$               | 0.352520046 <sup>b</sup> | 0.3413261(17) |
| $10^3 \alpha_e$     | 1.42365 <sup>b</sup>     | 1.5319(16)    |
| $10^6 \gamma_e$     | -2.9724 <sup>b</sup>     | -1.77(32)     |

**Notes.**

<sup>a</sup> All values are in  $\text{cm}^{-1}$

<sup>b</sup> Held fixed during fitting. Values from Dunham constants of Törring et al. (1988).

Liu & Parson (1977) have measured radiative lifetimes of  $34.2 \pm 1.5 \text{ ns}$  and  $35.5 \pm 1.2 \text{ ns}$  (at two wavelengths) for  $v = 0$ , and  $36.0 \pm 1.8 \text{ ns}$  and  $35.9 \pm 2.4 \text{ ns}$  for  $v = 1$  in the  $B^2\Sigma^+$  state by application of the laser-induced fluorescence technique. Later, Carette & Bencheikh (1994) determined the radiative lifetime of  $32 \pm 2 \text{ ns}$  for the  $v = 0$   $B^2\Sigma^+$  state. The calculated radiative lifetimes were low compared to the measurements carried out by Liu & Parson (1977) and Carette & Bencheikh (1994). Taking the average value to be  $33.9 \pm 2.8 \text{ ns}$  for  $v = 0$  compared to the calculated value of  $20.13 \text{ ns}$  for  $v = 0$  suggests that a correction factor of 0.77 be applied to the transition dipole moments of Table 5. With this correction, the lifetimes we calculate are given in Table 7. This correction factor is not unreasonable considering the difficulty in calculating the properties of heavy elements, and strictly applies to the 0–0 band. Its application to other bands, particularly to off-diagonal bands, is an assumption.

**Table 5**  
Band Strengths from LEVEL

| $\nu'/\nu''$ | 0                        | 1                        | 2         | 3         | 4                        | 5                        |
|--------------|--------------------------|--------------------------|-----------|-----------|--------------------------|--------------------------|
| 0            | 4.94309                  | 1.78918                  | 0.505466  | 0.116356  | $2.25885 \times 10^{-2}$ | $3.34618 \times 10^{-3}$ |
| 1            | -2.00225                 | 4.18192                  | 2.33711   | 0.8376475 | 0.226165                 | $4.75155 \times 10^{-2}$ |
| 2            | 0.545388                 | -2.64277                 | 3.45503   | 2.62842   | 1.12914                  | 0.341525                 |
| 3            | -0.106461                | 0.923692                 | -2.99886  | 2.76845   | 2.77356                  | 1.38171                  |
| 4            | $1.20215 \times 10^{-2}$ | -0.218389                | 1.27280   | -3.17634  | 2.13129                  | 2.82974                  |
| 5            | $1.1576 \times 10^{-3}$  | $3.13752 \times 10^{-2}$ | -0.354142 | 1.59862   | -3.20517                 | 1.55462                  |

**Note.** These band strengths should be multiplied by a correction factor of 0.77. All values are in debye.

**Table 6**  
Sample Line List for the B–X Transition

| $F'$ | $F''$ | Position ( $\text{cm}^{-1}$ ) | $E_{\text{up}}$ ( $\text{cm}^{-1}$ ) | $E_{\text{low}}$ ( $\text{cm}^{-1}$ ) | A ( $\text{s}^{-1}$ ) | Line Assignment   |
|------|-------|-------------------------------|--------------------------------------|---------------------------------------|-----------------------|---|
| 199  | 200   | 13451.4782                    | 30773.5841                           | 17322.1059                            | 2.168176              | pP1(199.5)199,200 : B $\nu = 0$ 198.5 198 File 199—X $\nu = 5$ 199.5 199 File 200 |
| 200  | 200   | 13451.4882                    | 30773.5941                           | 17322.1059                            | .0004978              | pP1(199.5)200,200 : B $\nu = 0$ 198.5 198 File 200—X $\nu = 5$ 199.5 199 File 200 |
| 198  | 199   | 13451.5029                    | 30773.5744                           | 17322.0715                            | 2.013565              | pP1(199.5)198,199 : B $\nu = 0$ 198.5 198 File 198—X $\nu = 5$ 199.5 199 File 199 |
| 199  | 199   | 13451.5126                    | 30773.5841                           | 17322.0715                            | .0005141              | pP1(199.5)199,199 : B $\nu = 0$ 198.5 198 File 199—X $\nu = 5$ 199.5 199 File 199 |
| 197  | 198   | 13451.5323                    | 30773.5649                           | 17322.0326                            | 1.831155              | pP1(199.5)197,198 : B $\nu = 0$ 198.5 198 File 197—X $\nu = 5$ 199.5 199 File 198 |
| 198  | 198   | 13451.5418                    | 30773.5744                           | 17322.0326                            | .0004662              | pP1(199.5)198,198 : B $\nu = 0$ 198.5 198 File 198—X $\nu = 5$ 199.5 199 File 198 |
| 196  | 197   | 13451.5689                    | 30773.5558                           | 17321.9869                            | 1.598742              | pP1(199.5)196,197 : B $\nu = 0$ 198.5 198 File 196—X $\nu = 5$ 199.5 199 File 197 |
| 197  | 197   | 13451.5781                    | 30773.5649                           | 17321.9869                            | .0003621              | pP1(199.5)197,197 : B $\nu = 0$ 198.5 198 File 197—X $\nu = 5$ 199.5 199 File 197 |

**Note:**  $F'$  and  $F''$  are the total angular momentum of the B and X states, respectively. Position is the line position in  $\text{cm}^{-1}$ .  $E_{\text{up}}$  and  $E_{\text{low}}$  are the energies of the B and X states in  $\text{cm}^{-1}$ . Einstein A coefficients in  $\text{s}^{-1}$  are given under A. Line assignment illustrates the transition  $^{\Delta N} \Delta J_{(F')F''}(J'')F', F'' : B \nu J' N' / F1p / F2p F' - X \nu J'' N'' / F1p / F2p F''$ .

(This table is available in its entirety in machine-readable form.)

**Table 7**  
Radiative Lifetimes of LaO in  $B^2\Sigma^+$ 

| $B^2\Sigma^+ \nu =$ | 0     | 1     | 2     | 3     | 4     |
|---------------------|-------|-------|-------|-------|-------|
| $\tau_n$ (ns)       | 33.90 | 34.42 | 34.94 | 35.63 | 38.97 |

## 6. Discussion

The energy levels for  $\nu = 0$  to  $\nu = 5$  for both the  $X^2\Sigma^+$  and  $B^2\Sigma^+$  states were determined. The origin determined by Bernard & Sibai (1980) for  $\nu = 0$  for the  $B^2\Sigma^+$  state is 17,837.345(30)  $\text{cm}^{-1}$  and for  $\nu = 1$  for the  $X^2\Sigma^+$  and  $B^2\Sigma^+$  states are 812.676(69)  $\text{cm}^{-1}$  and 18,567.613(69)  $\text{cm}^{-1}$ , respectively. Our values (Tables 1 and 2) for the same vibrational levels are the same within error.  $X^2\Sigma^+$  state equilibrium constants calculated by Bernard et al. (1999) are  $\omega_e = 817.0264(78) \text{ cm}^{-1}$ ,  $\omega_e x_e = 2.1292(24) \text{ cm}^{-1}$ , and  $\omega_e y_e = -0.00315(24) \text{ cm}^{-1}$ .  $B^2\Sigma^+$  state equilibrium constants calculated by Bernard et al. (1999) are  $\omega_e = 734.2811(87) \text{ cm}^{-1}$ ,  $\omega_e x_e = 1.9922(29) \text{ cm}^{-1}$ , and  $\omega_e y_e = -0.00354(32) \text{ cm}^{-1}$ . Our analysis was done with six vibrational levels in both  $X^2\Sigma^+$  and  $B^2\Sigma^+$ , and a three-parameter fit was selected as most reasonable. Our values are in satisfactory agreement with those of Bernard et al. (1999). Bernard et al. (1999) determined  $B_e = 0.34133169(95) \text{ cm}^{-1}$ , and  $\alpha_e = 0.00154227(34) \text{ cm}^{-1}$  for the  $B^2\Sigma^+$  state. These values agree with our analysis (Table 4). Higher  $J$  lines in the simulated spectrum are a little off from the observed spectrum and relatively few of the 5–5 band lines could be assigned. Overall the simulated spectrum matches the observed LaO B–X transition.

## 7. Conclusion

Spectroscopic constants for LaO were determined up to  $\nu = 5$  in both the  $B^2\Sigma^+$  and  $X^2\Sigma^+$  states. Three-parameter

equilibrium constants for X state and for the B state were calculated. These equilibrium constants were used to calculate RKR potentials. The RKR potentials were combined with an ab initio transition dipole moment function to calculate band strengths, which were corrected using experimental lifetimes. PGOPHER provided the final line list for the  $B^2\Sigma^+ - X^2\Sigma^+$  band system. The line list can be used to simulate LaO spectra of cool S stars to determine La abundances.

The National Solar Observatory (NSO) is operated by the Association of Universities for Research in Astronomy, Inc. (AURA), under cooperative agreement with National Science Foundation. Financial support was provided by the NASA Laboratory Astrophysics Program (80NSSC21K1463). J.L. thanks the Consortium des Equipements de Calcul Intensif (CECI), funded by the Fonds de la Recherche Scientifique de Belgique (F.R.S.-FNRS) under grant No. 2.5020.11 and by the Walloon Region, for computational resources.

*Software:* PGOPHER (Western 2017), RKR (Le Roy 2017a), LEVEL (Le Roy 2017b), Excel (Microsoft), Wolfram Mathematica.

## ORCID iDs

P. F. Bernath  <https://orcid.org/0000-0002-1255-396X>  
R. Dodangodage  <https://orcid.org/0000-0003-4814-4970>

## References

- Bacis, R., Collomb, R., & Bessis, N. 1973, PhRvA, 8, 2255  
Bernard, A., & Sibai, A. 1980, ZNA, 35, 1313  
Bernard, A., Taher, F., Topouzhanian, A., & Wannous, G. 1999, A&AS, 139, 163  
Bernard, A., & Vergès, J. 2000, JMoSp, 201, 172

- Bernath, P. F. 2020, *Spectra of atoms and molecules* (New York: Oxford Univ. Press)
- Brown, J. M., & Carrington, A. 2003, *Rotational spectroscopy of diatomic molecules* (Cambridge: Cambridge Univ. Press)
- Carette, P., & Bencheikh, M. 1994, *JMoSp*, **163**, 309
- Childs, W., Goodman, G., Goodman, L., & Young, L. 1986, *JMoSp*, **119**, 166
- Dagdikian, P. J., Cruse, H. W., & Zare, R. N. 1974, *JChPh*, **60**, 2330
- Darwent, B. 1970, *Bond Dissociation Energies in Simple Molecules*, National Standard Reference Data System, <https://nvlpubs.nist.gov/nistpubs/Legacy/NSRDS/nbsnrsds31.pdf>
- Dolg, M., Stoll, H., Savin, A., & Preuss, H. 1989, *AcTC*, **75**, 173
- Dunning, T. H., Jr 1989, *JChPh*, **90**, 1007
- Frosch, R. A., & Foley, H. 1952, *PhRv*, **88**, 1337
- Ji, A. P., Drout, M. R., & Hansen, T. T. 2019, *APJ*, **882**, 40
- Johnson, J. A. 2019, *Sci*, **363**, 474
- Kendall, R. A., Dunning, T. H., & Harrison, R. J. 1992, *JChPh*, **96**, 6796
- Knowles, P. J., & Werner, H.-J. 1985, *CPL*, **115**, 259
- Knowles, P. J., & Werner, H.-J. 1988, *CPL*, **145**, 514
- Korek, M., El-Kork, N., Moussa, A., & Bentiba, A. 2013, *CPL*, **575**, 115
- Langhoff, S. R., & Davidson, E. R. 1974, *IJQC*, **8**, 61
- Le Roy, R. J. 2017a, *JQSRT*, **186**, 158
- Le Roy, R. J. 2017b, *JQSRT*, **186**, 167
- Liu, K., & Parson, J. 1977, *JChPh*, **67**, 1814
- MacConnell, D. J., Wing, R. F., & Costa, E. H. 2000, *PASP*, **112**, 65
- Moriyama, H., Watanabe, Y., Nakano, H., Yamamoto, S., & Tatewaki, H. 2010, *JChPh*, **132**, 124310
- Neyskens, P., Van Eck, S., Jorissen, A., et al. 2015, *Natur*, **517**, 174
- Schamps, J., Bencheikh, M., Barthelat, J.-C., & Field, R. W. 1995, *JChPh*, **103**, 8004
- Steimle, T., & Virgo, W. 2002, *JChPh*, **116**, 6012
- Suenram, R., Lovas, F., Fraser, G., & Matsumura, K. 1990, *JChPh*, **92**, 4724
- Törring, T., Zimmermann, K., & Hoefl, J. 1988, *CPL*, **151**, 520
- Wallerstein, G., Iben, I., Parker, P., et al. 1997, *RvMP*, **69**, 995
- Weigand, A., Cao, X., Yang, J., & Dolg, M. 2009, *Theor. Chem. Acc.*, **126**, 117
- Weltner Jr, W., McLeod Jr, D., & Kasai, P. d. 1967, *JChPh*, **46**, 3172
- Werner, H.-J., Kállay, M., & Gauss, J. 2008, *JChPh*, **128**, 034305
- Werner, H.-J., & Knowles, P. J. 1985, *JChPh*, **82**, 5053
- Werner, H.-J., & Knowles, P. J. 1988, *JChPh*, **89**, 5803
- Werner, H.-J., Knowles, P. J., Knizia, G., et al. 2019, MOLPRO, v.2019.2, <https://www.molpro.net>
- Werner, H.-J., Knowles, P. J., Knizia, G., Manby, F. R., & Schütz, M. 2012, *Wiley Interdiscip. Rev. Comput. Mol. Sci.*, **2**, 242
- Western, C. M. 2017, *JQSRT*, **186**, 221